atmosphere

MDPI

Article

Kolmogorov Complexity Analysis and Prediction Horizon of the Daily Erythemal Dose Time Series

Slavica Malinović-Milićević [1,*], Anja Mihailović [2] and Dragutin T. Mihailović [3]

[1] Geographical Institute "Jovan Cvijić", Serbian Academy of Sciences and Arts, 11000 Belgrade, Serbia
[2] Faculty of Technical Sciences, University of Novi Sad, 21000 Novi Sad, Serbia; mihailovic.dt2.2020@uns.ac.rs
[3] Department of Physics, Faulty of Sciences, University of Novi Sad, 21000 Novi Sad, Serbia; guto@df.uns.ac.rs
* Correspondence: s.malinovic-milicevic@gi.sanu.ac.rs; Tel.: +381-64-161-0445

Abstract: Influenced by stratospheric total ozone column (TOC), cloud cover, aerosols, albedo, and other factors, levels of daily erythemal dose (H_{er}) in a specific geographic region show significant variability in time and space. To investigate the degree of randomness and predictability of H_{er} time series from ground-based observations in Novi Sad, Serbia, during the 2003–2012 time period, we used a set of information measures: Kolmogorov complexity, Kolmogorov complexity spectrum, running Kolmogorov complexity, the largest Lyapunov exponent, Lyapunov time, and Kolmogorov time. The result reveals that fluctuations in daily H_{er} are moderately random and exhibit low levels of chaotic behavior. We found a larger number of occurrences of deviation from the mean in the time series during the years with lower values of H_{er} (2007–2009, 2011–2012), which explains the higher complexity. Our analysis indicated that the time series of daily values of H_{er} show a tendency to increase the randomness when the randomness of cloud cover and TOC increases, which affects the short-term predictability. The prediction horizon of daily H_{er} values in Novi Sad given by the Lyapunov time corrected for randomness by Kolmogorov is between 1.5 and 3.5 days.

Keywords: erythemal dose; Novi Sad (Serbia); Kolmogorov complexity-based measures; chaos; largest Lyapunov exponent; Lyapunov time; Kolmogorov time; predictability

Citation: Malinović-Milićević, S.; Mihailović, A.; Mihailović, D.T. Kolmogorov Complexity Analysis and Prediction Horizon of the Daily Erythemal Dose Time Series. *Atmosphere* **2022**, *13*, 746. https://doi.org/10.3390/atmos13050746

Academic Editor: Jihui Yuan

Received: 6 April 2022
Accepted: 4 May 2022
Published: 6 May 2022

1. Introduction

The detection of the large depletion of stratospheric ozone over Antarctica almost 40 years ago [1] initiated increased public and scientific interest in the state of stratospheric ozone levels and variability of UV radiation. According to the definition by the International Commission on Illumination [2], UV radiation is classified into three primary types: the UV-C range (100–280 nm), UV-B range (280–315 nm), and UV-A range (315–400 nm). While UV-C radiation is absorbed by atmospheric oxygen and ozone in the upper atmosphere and does not reach the surface, UV-B radiation may increase by as much as about six orders of magnitude due to the interaction with the stratospheric ozone [3]. Ozone depletion occurs not only over Antarctica but also in mid-latitudes [4,5]. Petkov et al., 2021 [6] conducted a brief survey of the ozone column over central Europe during spring 2020 and verify the hypothesis about the effect of the strong ozone depletion event that occurred in the Arctic on the ozone column at lower latitudes. The identification of ozone depletion led to the establishment of the Montreal Protocol in 1987, and its implementation has significantly limited the production of ozone-depleting substances. Mitigation activities over the last three decades have contributed to the successful reduction in ozone layer depletion and the associated increase in terrestrial UV radiation [7]. However, despite the success of the Montreal Protocol and the stabilization of stratospheric ozone levels, UV levels in many regions of the world remain high. Several studies at mid-northern latitudes (35–55° N) reported positive trends in UV radiation, while those associated with high northern latitudes (55–70° N) reported a decrease in UV radiation [8]. For example, Eleftheratos et al. [9] analyzed UV radiation at selected sites located at high latitudes of both hemispheres in the period 1990–2011 and found a significant decrease in UV irradiance at 305 nm and no significant long-term trend at 325 nm. However, Fountoulakis et al. [10] reported increases in annual average UV irradiance in Thessaloniki, Greece, of 2–6% per decade for the period 1994–2014, while Sanchez-Lorenzo et al. [11] reported an increase of 2 Wm^{-2} per decade over Central and Eastern Europe for the period 1983–2010. For certain areas in northern mid-latitudes (Canada, Europe, and Japan), Zerefos et al. [12] revealed positive trends in UV-B radiation in the period 1995–2006, while De Block et al. [13] reported an increase in erythemally weighted irradiance over the 1991 to 2013 period at Uccle, Belgium, which is contrary to the observed positive trends in total ozone.

Influenced by stratospheric total ozone column (TOC), cloud cover, aerosols, albedo, as well as the combined effect of geographical and astronomical factors such as solar zenith angle, the Sun–Earth distance, the altitude, and the solar activity, UV radiation levels in a specific geographic region show significant variability in time and space. The variation of these influencing elements in the context of a changing global climate is an important issue regarding the complexity of the UV radiation series. Gaps in our knowledge of the links between stratospheric ozone, UV radiation, and climate change and their implications for terrestrial ecosystems are a direct consequence of the complexity of systems characterized by interactive loops linking climatology, meteorology, and biology [14]. Climate change is affecting and changing cloud cover, with some regions becoming more cloudy and others less cloudy [15]. Increased cloud cover generally reduces solar UV radiation on the Earth's surface, where the effect depends on the type of the cloud and wavelength. However, clouds can also increase the level of UV radiation during partly cloudy conditions when the sun is not obstructed, due to multiple scattering between upper and lower clouds [16]. Atmospheric aerosols absorb and scatter UV radiation, depending on the aerosol type and amount, which are affected by human emissions, volcanic activity, wildfires, dust storms, and other factors that are affected by climate change [17,18]. High surface albedo from snow or ice-covered surfaces can increase the intensity of the solar UV radiation by up to 20–30% [19,20]. However, the reduction in ice or snow cover caused by climate change reduces the reflection of UV radiation from the surface resulting in reduced UV radiation. The results presented above reveal that the impact of changes in TOC on the intensity of UV radiation reaching the Earth's surface is greater at higher latitudes. In mid-latitudes besides the TOC levels, the effects of other parameters such as cloud cover, aerosols, and albedo may be very high and may even predominantly control UV levels. For example, Fountoulakis et al. [21] compared UV levels in Rome and Aosta and found a significant effect of aerosols, clouds, and surface albedo on the spectral UV levels at each location. Fountoulakis et al. [22] revealed that in the period 2006–2020 the levels of UV irradiance in the Italian cities Aosta, Rome, and Lampedusa generally increased due to changes in clouds and/or aerosols. Therefore, the space and time variability of solar UV radiation is very complex and its forecast is still challenging.

Due to the highly variable climate change-driven effects on UV radiation levels, it is useful to gain a deeper insight into the complexity of UV radiation processes. To understand the characteristics of daily erythemal dose time series (H_{er}) and the patterning of their complexity, it is required to use various information measures that can improve the application of the stochastic process concept in the modeling and measurement of UV radiation. Entropy-based measures are useful in providing large-scale estimates of randomness, but they are sensitive to the structure of the information and are therefore as rough as the complexity indices [23]. Shannon's entropy [23] is used for measuring the unpredictability of specific output, while cluster analysis and Principal Components Analysis are important tools for characterizing of time series analysis of complex systems and assessing relationships in the data [24]. One of the widely used information measures in science to examine the complexity of data is Kolmogorov complexity (KC) [25]. Kolmogorov defined the descriptive complexity of an object as the length of the shortest computer program used to describe the object. Kolmogorov complexity is a measure of randomness that, unlike entropy, is not probability-based [26]. It is a general measure of randomness in a sequence that gives a degree of regularity or irregularity in a set of binary numbers and how much the information is compressible [24]. Several information measures offering additional insight into the behavior of complex systems were derived from Kolmogorov complexity (KC spectrum, KC spectrum highest value, overall KC, and Kolmogorov time) [27]. The KC and its derivatives have proven to be reliable tools for quantification of complexity and predictability of global and UV radiation time series [28–31].

The purpose of this study is to investigate the degree of randomness and predictability of daily H_{er} time series from ground-based observations in Novi Sad, Serbia, during the 2003–2012 time period using the set of information measures: Kolmogorov complexity (KC), Kolmogorov complexity spectrum, Running Kolmogorov complexity (RKC), the largest Lyapunov exponent (LLE), Lyapunov time (LT), and Kolmogorov time (KT). The study is organized as follows. Section 2 describes measurement sites and an overview of complexity measures. Section 3 includes both presentations of the results obtained and a discussion of daily H_{er} time series using mentioned information measures. The concluding remarks are given in Section 4.

2. Materials and Methods

2.1. Study Area and Data

The measurements used in this study were recorded in the city of Novi Sad situated in the northern part of the Republic of Serbia between April 2003 and December 2012. Serbia is a continental country located in south-eastern Europe, in the center of the Balkan Peninsula. Novi Sad is located in the northern part of the country, in the Autonomous province of the Vojvodina, which is in Central Europe. Vojvodina encompasses the southern part of the Pannonian Plain (44°37′–46°11′ N, 18°51′–21°33′ E and 75–641 m above sea level), with Fruška Gora mountain to the South. The province is the main food production area in Serbia, with a total surface area of 21,500 km^2 and 2 million inhabitants. It has a continental climate that is strongly influenced by air masses coming from the north and west, increasing the continentality of the Vojvodina climate, especially in winter and summer. According to Beck et al. [32], the Köppen–Geiger climate formula for Novi Sad is "Cfa" where C = temperate climate, f = without dry seasons, and a = hot summer. The average temperature in Novi Sad over 30 years period 1981–2010 was 11.47 °C (in January 0.18 °C; in July 21.93 °C, the standard deviation of the monthly mean air temperature data is 7.72 °C), while the mean rainfall was 647.31 mm (maximum in June 91.36 mm, minimum in February 31.39 mm, the standard deviation of the monthly mean rainfall data is 38.04 mm).

The target parameter in this study is the daily erythemal dose (H_{er}). The erythemal dose, H_{er} (in Jm^{-2}), received after an exposure period of t (in s) is shown in [33]:

$$H_{er} = E_{er} t \tag{1}$$

where E_{er} is the erythemal irradiance (in Wm^{-2}). The erythemal irradiance, E_{er}, is obtained by weighting the spectral irradiance of the radiation at wavelength λ (in nm) by the effectiveness of radiation of this wavelength to cause minimal erythema and summing over all wavelengths present in the source spectrum [33]:

$$E_{er} = \int E(\lambda) s_{er}(\lambda) d\lambda \tag{2}$$

where $E(\lambda)$ is the spectral irradiance at wavelength λ, $s_{er}(\lambda)$ is the erythema spectral weighting function normalized to 1 at its maximum, and $d\lambda$ is the wavelength interval. The erythema spectral weighting function, $s_{er}(\lambda)$, assesses the potential of UV radiation to induce sunburn (erythema) in human skin and it is highly dependent upon the radiation wavelength. It is usually expressed as unit-less quantity UV index (UVI) [34,35]:

$$\mathrm{UVI} = k_{er} E_{er} \tag{3}$$

where $k_{er} = 40\ \mathrm{m^2W^{-1}}$.

The measurements of UVI are recorded by a broadband Yankee UV-B1 biometer [36]. It is placed at the university campus in Novi Sad (at 45.33° N, 19.85° E, and 84 m above sea level). It measures UV radiation every 30 s, while data are recorded as a mean over 10-min time intervals. The instrument approximates the spectral response of the human skin to UV radiation by multiplying the output voltage by a conversion function given by the manufacturer, corrected only for the SZA at the time samples are taken [33,37]. The relative spectral response of the instrument was checked in laboratory conditions (Laboratory for plasma spectroscopy, Department of physics, Novi Sad) and found to be in good agreement with the declared spectral response. The angular response was not checked but assumed to be as declared by the producer [36]. The analog signal from the output of the instrument was digitized using a 16-bit A/D converter and then transferred to a PC, where is processed and converted to physical unit $\mathrm{Wm^{-2}}$ and UVI. The instrument was calibrated by the manufacturer in 2007, while after that period procedure for a long-term stability check procedure was applied once a year [38]. No significant deviation of the instrument values has been noticed, confirming the long-term stability stated by the manufacturer (the long-term deviation of the output voltage is less than 100 ppm/year) [36,39]. Since there are no other radiometers in Serbia, "national intercomparison" was not possible in the way that it is performed in other countries, for example, Italy [40]. Taking into account the calibration uncertainty reported in [41] for an SZA of less than 65°, the total uncertainty of the results was estimated to be <6%. Daily H_{er} values in Novi Sad are calculated by integrating 10 min measurements from sunrise to sunset. For further processing, we used measured values for days when more than 80% of 10-min daily values were available. To fill in the gaps in measured daily H_{er}, an empirical reconstruction technique based on the parametric numerical model NEOPLANTA is used. The NEOPLANTA model is described in detail in Malinovic et al. [42], while the reconstruction technique is described in [39,43].

Data on TOC values for the period 2003–2012 were used from Ozone Multi-Sensor reanalysis, version 2 (MSR-2) [44,45]. MSR-2 is a multi-decade TOC data record constructed using all available satellite datasets, Brewer–Dobson surface observations, and data assimilation techniques with detailed error modeling [44]. It provides global time series of TOC in the resolution of 0.5° × 0.5° and with a time interval of 6 h. An assessment of the quality of the MSR-2 data showed that the mean bias of the MSR-2 analysis was less than 1% in comparison with satellite observations without bias after 1979 [44].

The daily data on cloud cover represents the measurement at the nearest meteorological station Rimski Sancevi, which is located 8.5 km north of the location of the Yankee UV-B biometer and, it was provided by the Serbian Meteorological Service.

2.2. Complexity Measures

Kolmogorov complexity is often applied in the analysis of physical time series obtained by measurement or modeling. It is elementally described in [46], while its comprehensive description can be found in [47]. Unlike entropy, KC characterizes the amount of randomness present in individual strings using the algorithm to quantify the randomness. The algorithm is used in encoding data, and it refers to the minimum length of a program such that a universal computer can generate a specific sequence. Based on Kolmogorov's idea, Ziv and Lempel [48] developed a widely used tool for computing this complexity based on symbolic dynamics. If we denote measurements of the H_{er} as $X\ (x_1, x_2, x_3, \ldots x_N,)$, KC computation begins by encoding X with the Lempel–Ziv algorithm into binary time series by replacing X with new time series S according to the threshold x_T as:

$$S(x_i)\begin{cases} 0\ x_i < x_T \\ 1\ x_i \geq x_T \end{cases}. \tag{4}$$

The threshold can be determined in different ways, but the time series mean value is commonly used. Next, in the binary time series, we search for the total possible subset sequences that differ from each other. The number of subsets that do not match represents the complexity of the series. Therefore, the complexity counter $\mathrm{C(N)}$ involved in the binary template $S(x_i)$ is increasingly proportional to randomness. The $\mathrm{C(N)}$ is defined as the minimum number of distinct patterns contained in a given character sequence. The $\mathrm{C(N)}$ is a function of the length of the sequence N (when the length N of the binary series tends to infinity, the number $\mathrm{C(N)}$ tends to reach its limit, i.e., $\mathrm{b(N)} = \mathrm{N}/\log_2 \mathrm{N}$). Finally, the normalized information measure $\mathrm{KC(N)}$ is calculated, which is defined as $\mathrm{KC(N)} = \mathrm{C(N)}/\mathrm{b(N)} = \mathrm{C(N)}\log_2 \mathrm{N}/\mathrm{N}$. KC varies between 0 and 1 although it can be larger than 1 [49]. Using the calculation procedure outlined above, we calculated KC for H_{er}, TOC, and cloud cover. The calculations were performed for the entire period between April 2003 and December 2012 and on an annual basis. The mean value of the time series was selected as the threshold. We also calculated the running complexity (RKC) of the time series by creating the series of averages of different subsets of the complete data sets which is a type of finite impulse response filter. From the used data series, we extracted a fixed window (size 100) and then applied the KC calculation procedure. Next, the window is moved one step forward, and the KC algorithm is applied until the time series ends [24].

According to Mihailović et al. [27], the disadvantages of KC are its dependence on the rules of the applied procedure of conversion of time series into a binary string and the fact that it does not differentiate between time series with different oscillations of amplitude and similar random components. To overcome this weakness and offer further insight into the behavior of complex systems, Mihailović et al. [27] introduced two new aforementioned measures based on the Kolmogorov complexity: Kolmogorov complexity spectrum (KC spectrum) and the Kolmogorov complexity spectrum highest value (KCH). The KC spectrum was introduced to take into account sensitivity to the threshold value used to encode the time series. It allows us to investigate the range of amplitudes in a time series that is a complex system with highly improved stochastic components. The KC spectrum explicitly describes the complexity of the time series of each element in the time series that contributes to the overall physical process from which the physical time series comes [28]. The shape of the complexity spectrum curve depends on the variability of time series amplitudes that cannot be captured by the KC, increasing the information "that is stored in a sequence about a particular environment" [50]. For a large number of time series samples calculating the KC spectrum can be computationally challenging; therefore, to calculate the KC spectrum, we first divided the amplitude of the time series into K subintervals. Next, we stored the assigned amplitude threshold values. Then, we encoded the time series for different threshold values taken in the threshold set, and we calculated a set of K KC values that represent the KC spectrum. The highest value of the KC spectrum is represented by the KCH. The KCH is used to estimate the discrepancy between the time-series average used as the time series coding threshold and the optimal threshold [29]. Mihailovic et al. [27] demonstrated the meaning of the KCH in more detail suggesting that KCH is a better indicator of the complexity of the time series than the commonly used KC since KCH carries the information about the highest complexity among all complexities in the Kolmogorov complexity spectrum (unlike KC that carries average information about the time series).

The Lyapunov exponent of a dynamical system is a measure of the system's sensitivity to changes in its initial conditions that can detect the presence of chaos. It presents the rate of separation with the time of initially close trajectories in parameter space [51]. Since the separation rate may be different for different orientations of the initial separation vector, there is a spectrum of Lyapunov exponents whose highest value is usually called LLE. In this study, the Rosenstein algorithm [52], which was implemented in the MATLAB program through a function named "lyapunovExponent", was applied to obtain LLE for daily H_{er} time-series. The MATLAB built-in code is fast, easy to apply, and noise-robust [53]. The $\mathrm{LLE} = 0$ implies linear divergence. $\mathrm{LLE} < 0$ implies that trajectories converge, so the initial separation between two points will decrease in time, and therefore the system is not chaotic. If $0 < \mathrm{LLE} < 1$ we have a very sensitive dependence on initial conditions, i.e., chaos, as points initially close together will diverge exponentially along neighboring trajectories.

The Lyapunov exponent refers to the predictability of measured time series involving deterministic chaos as an inherent component. The predictability of the model is here understood as the degree to which an accurate prediction of the state of a system can be made either qualitatively or quantitatively [54]. In stochastic analysis, a random process is considered predictable if it is possible to conclude the following state from previous observations. Deterministic chaos does not imply complete predictability, but that it improves prognostic power, at least. In contrast, stochastic trajectories cannot be projected into the future. We also point out a one-time scale called prediction horizon: the Lyapunov time $LT = 1/LLE$ [55], where LLE is the largest positive Lyapunov exponent. It is a period after which a dynamical system becomes unpredictable and enters a chaotic state, so it indicates the limits of predictability. If LT increases when $LLE \to 0$, then long-term accurate predictions are possible. Research suggested that LLE overestimates the actual value of the period. To correct this overestimation, Mihailović et al. [54] introduce the Kolmogorov time $KT = 1/KC$, where KC is the Kolmogorov complexity. This time quantifies the size of the time window within which complexity remains unchanged. Hence, the presence of a narrow window KT significantly reduces the length of the effective prediction horizon.

3. Results and Discussion

3.1. General Features of the Data

The basic descriptive statistics of daily H_{er} for different years are summarized in Figure 1, where averages, median, minimum, maximum, and interquartile ranges are indicated for each year. To detect anomalies in H_{er} data AnomalyDetection package in R was used [56]. No anomalies were detected in the data. It is seen from Figure 1 that the differences between the mean and the median were in the range of roughly 200 Jm^{-2} and 500 Jm^{-2} indicating a positively skewed distribution.

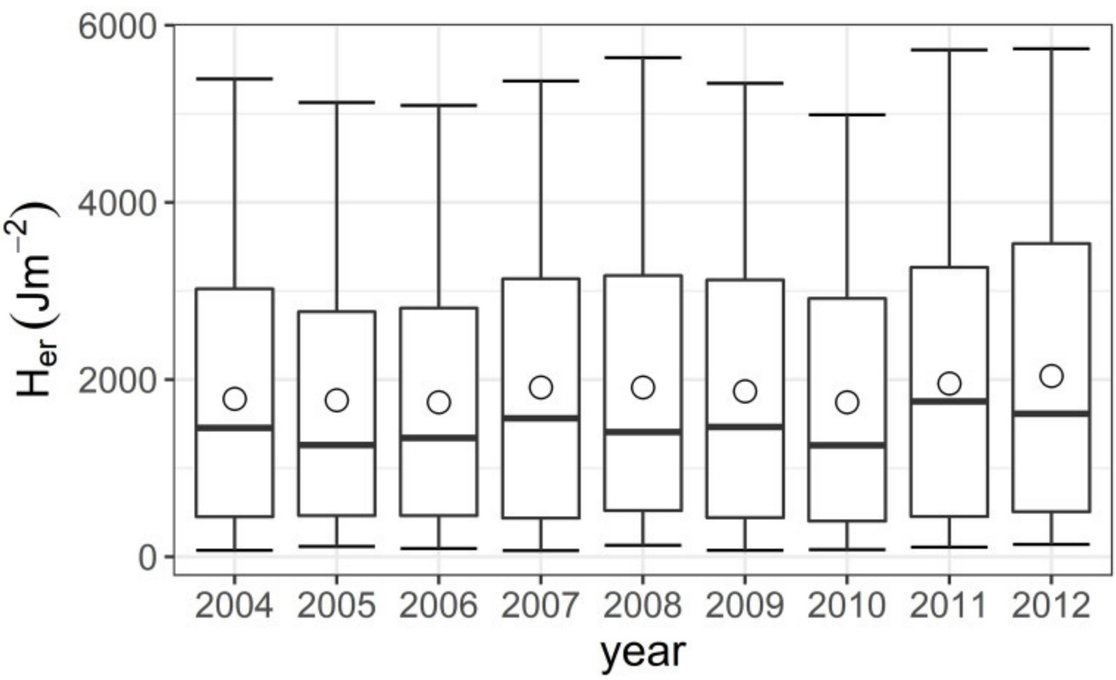

Figure 1. Boxplot of the daily H_{er} in Novi Sad for the period 2003–2012 (the box represents 50% of the central data, with a line inside that represents the median; the edges of the box are the first and the third quartile; the whiskers are minimum and maximum values; the dots represent the mean).

Figure 2 depicts the frequency distribution of daily H_{er} over the entire observed period. The highest frequency distribution of the observed data was for values in the range of 100 to 1100 Jm^{-2} (~40% of all data). Data in this range are typically recorded in the cold period of the year (October–March) and occasionally in the hot period of the year (April–September) under cloud conditions. Extremely low (<100 Jm^{-2}) and high (>5000 Jm^{-2}) values occur very rarely, about 2% of all data.

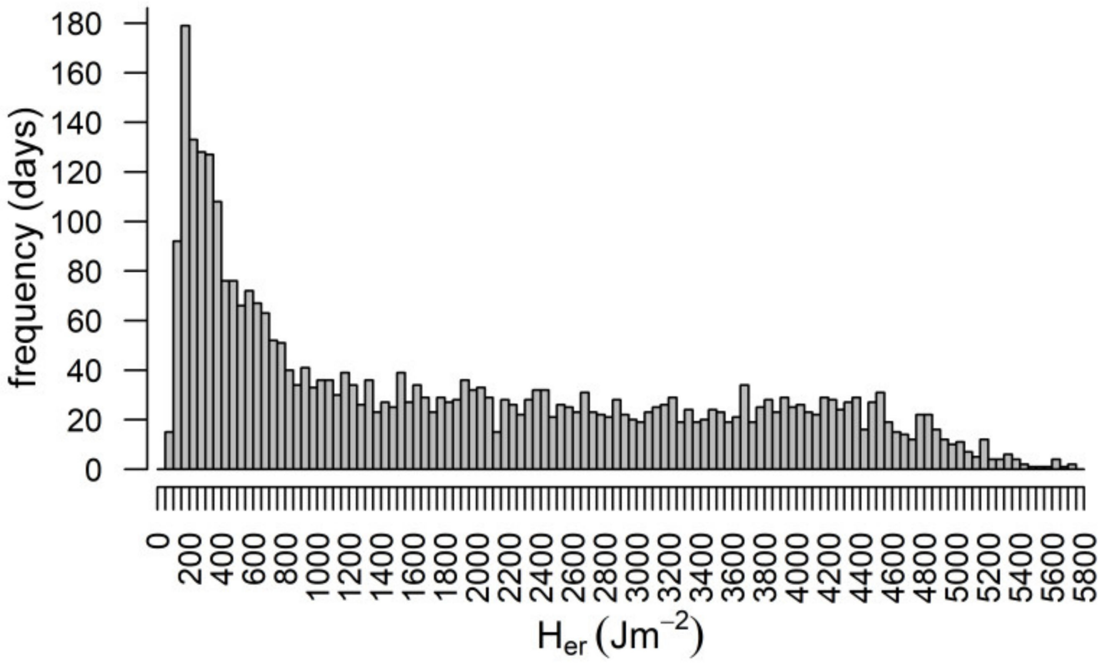

Figure 2. Frequency distribution of the daily H_{er} in Novi Sad for the period 2003–2012.

Figure 3 shows the evolution of the daily (black), monthly (red), and yearly average (blue) of H_{er} (Jm^{-2}), TOC (DU), and cloud cover (tenths) in Novi Sad, Serbia, for the period 2003–2012. The curves of the daily and monthly H_{er} show a sinusoidal evolution, with minimum monthly values in January and December that range between 189 Jm^{-2} in December 2004 and 233 Jm^{-2} in January 2008. Monthly maximum H_{er} values ranged between 3358 Jm^{-2} in June 2006 and 4582 Jm^{-2} in June 2012. Daily H_{er} values ranged between 68 Jm^{-2} recorded on 12 December 2007, and 5733 Jm^{-2} on 16 June 2012. As expected, TOC values were the highest in March and April (ranged between 327 DU in April 2011, and 392 DU in April 2010), and the lowest in October and November (ranged between 277 DU in November 2011, and 309 DU in October 2010). The lowest daily TOC of 227 DU was recorded on 25 December 2012. The lowest cloud cover was in July and August (ranged from 1.61 tenths in August 2012 to 5.06 tenths in August 2006), while the highest was in December in January (ranged from 4.97 in December 2003 to 8.71 in December 2010).

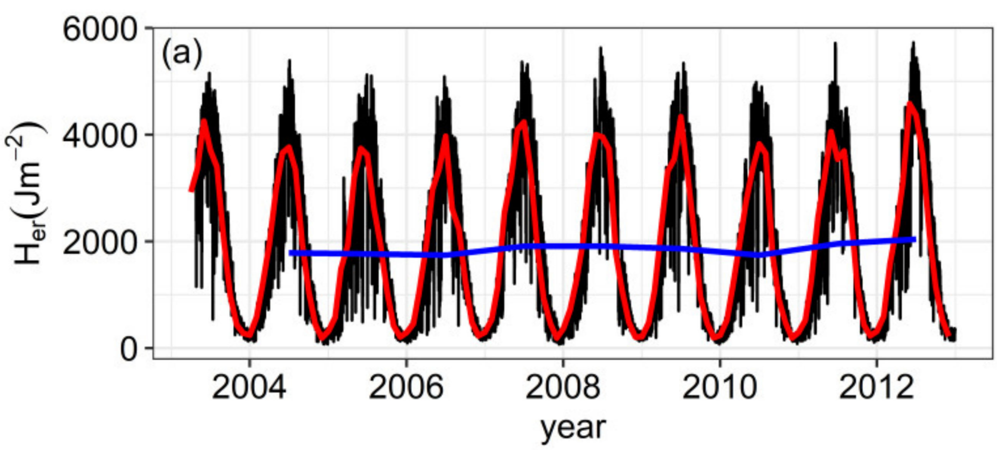

Figure 3. *Cont.*

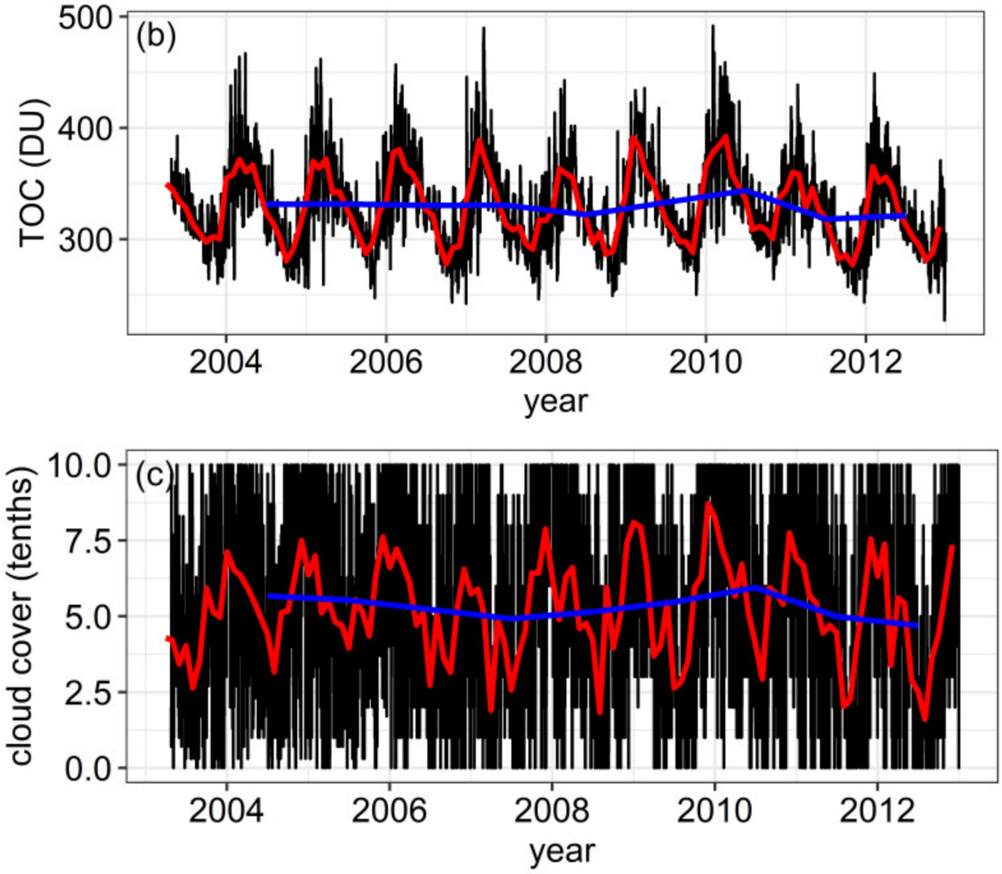

Figure 3. Evolution of the daily (black), monthly (red), and yearly average (blue) (**a**) H_{er} (Jm^{-2}); (**b**) TOC (DU); and (**c**) cloud cover (tenths) in Novi Sad, Serbia, for the period April 2003–December 2012.

To analyze the temporal evolution of the time series of the parameters we used the non-parametric Mann–Kendall test and Sen's slope estimator [57–59]. The Mann–Kendall test is robust to the influence of extremes and does not require an assumption of normality. The magnitude of the trend has been quantified by Sen's slope estimator. In this study, the trend is significant at a 5% significance level. Although there is no statistically significant annual trend in the daily values of any of the parameters in the observed period, there are significant monthly trends. Daily H_{er} had a statistically significant positive annual trend in March, April, and August of +3.01%, +1.96%, and +1.52% per year, respectively. Daily values of TOC had statistically significant negative annual trend in March, April, June, July, August, and November from (−0.31% in July to −0.68% in August) and a positive trend in December (+0.45%). Cloud cover showed a statistically significant decrease of 5.4%, only in August.

To evaluate the variability of the measured data, we calculated the coefficient of variation (CV, %) at the monthly level as the ratio of standard deviation to mean (Figure 4). The highest CV had cloud cover (24.48–122.44%), with maximum monthly values over the April–October period. The lowest CV had TOC (2.70–15.70%), with peak monthly values during the winter. CV of the H_{er} varied in the range of 16.04–65.58%, with the highest values occurring during the cold period of the year (October to March).

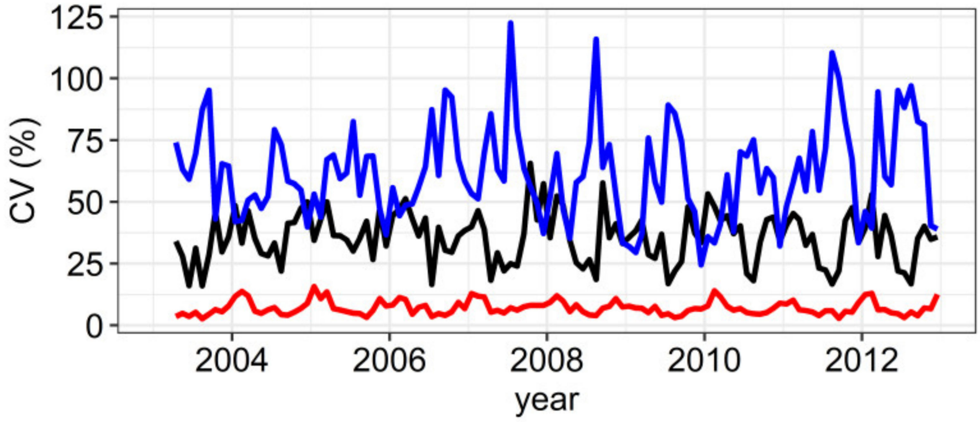

Figure 4. Monthly coefficient of variation (CV, %) of daily values of H_{er} (black), TOC (red), and cloud cover (blue) in Novi Sad, Serbia, for the period April 2003–December 2012.

3.2. Kolmogorov Complexity and Kolmogorov Complexity Spectrum

The Kolmogorov complexity measures applied in this paper provide additional insight into the complex behavior and randomness of daily H_{er} time-series and their influencing factors. Thus, the value of the KC close to zero is associated with less complex deterministic processes, while a value close to one indicates a complex stochastic process. In the real world, UV irradiation that is received at the surface is mainly related to the cloud cover activity in the lower troposphere and the formation and destruction of ozone in the stratosphere. The values of KC of daily H_{er}, TOC, and cloud cover data are shown in Table 1 which shows that the KC values for all daily H_{er} were moderate, ranging from 0.279 to 0.583. KC of TOC has some higher values, ranging from 0.558 to 0.745, while cloud cover exhibits very high complexity ranging in the narrow interval (from 0.861 to 1.048). A simple inspection of the KC complexity in Table 1 indicates higher complexity over the 2004–2006 period and low complexity over the 2007–2008 period. The higher complexity of daily H_{er} in 2004 and 2005 can be attributed to unusually high cloud cover in the summer period (Figure 3c), while in 2006 the reason can be the higher variability in summer cloud cover and low TOC values in autumn (Figure 3b,c). The lowest complexity of daily H_{er} was in 2008 (0.279) when spring TOC values and summer cloud cover were lower than usual.

Table 1. Kolmogorov complexity (KC) of daily H_{er}, TOC, and cloud cover time series in Novi Sad.

Year	Kolmogorov Complexity (KC)		
	H_{er}	TOC	Cloud Cover
2003	0.445	0.572	1.048
2004	0.512	0.558	0.954
2005	0.583	0.676	0.933
2006	0.536	0.676	0.956
2007	0.373	0.723	0.909
2008	0.279	0.605	0.907
2009	0.396	0.560	0.886
2010	0.420	0.630	0.933
2011	0.350	0.560	0.863
2012	0.421	0.745	0.861

To examine changes in complexity as a function of time over the considered period, we computed running KC complexities of H_{er}, TOC, and cloud cover over a window size of 100 (which roughly corresponds to a 3-month interval). The analysis was carried out by converting time series into binary form via the mean threshold value. As can be seen in Figure 5, the RKC declined sharply up to the summer of 2007 (window position, w.p., 1500). Low values remained until the beginning of 2009 (w.p. 2100), which was followed by a slight increase in RKC until mid-2012 (w.p 3300). The overall RKC of the TOC has shown a decline up to mid-2012. However, the RKC of TOC has shown seasonal variability, increasing in the cold period of the year and decreasing in the hot period of the year. The RKC of cloud cover declined until the beginning of 2012, without visible seasonal variability. During the last half-year of the observed period, there is a decrease in RKC of H_{er} and an increase in RKC of TOC and cloud cover.

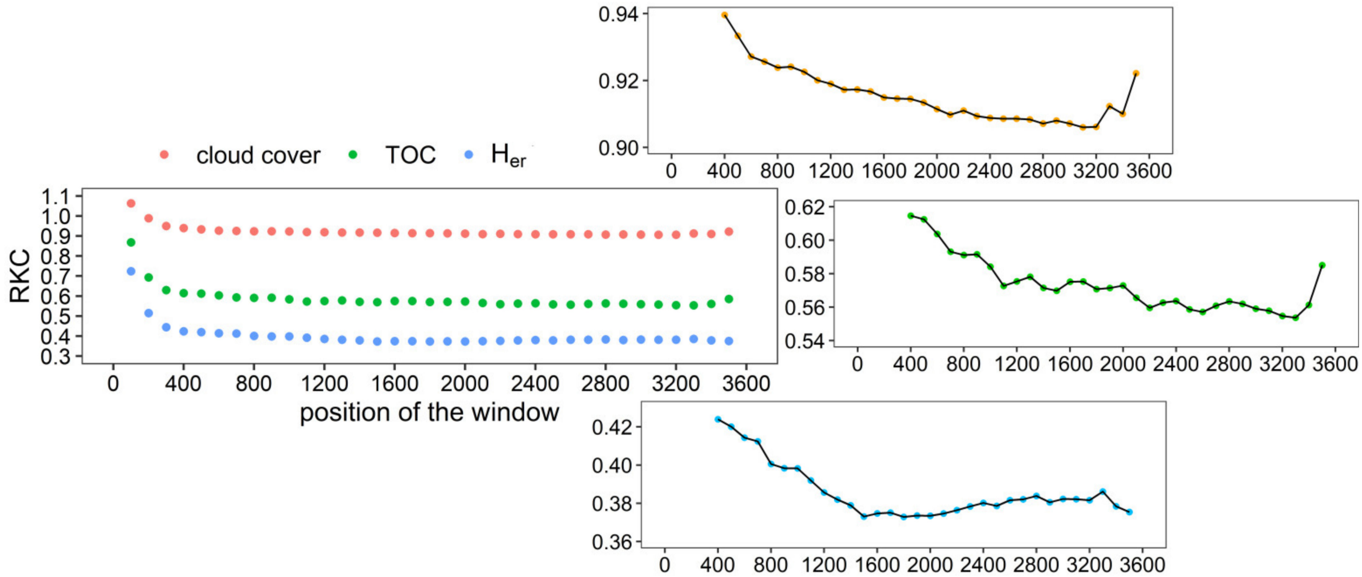

Figure 5. The running KC (RKC) time series for H_{er} (blue), TOC (green), and cloud cover (orange) for a fixed window of 100.

Dependence RKC of H_{er} from RKC of TOC and cloud cover is shown in Figure 6. It is visible that an increase in RKC of TOC and cloud cover increases the RKC of H_{er}.

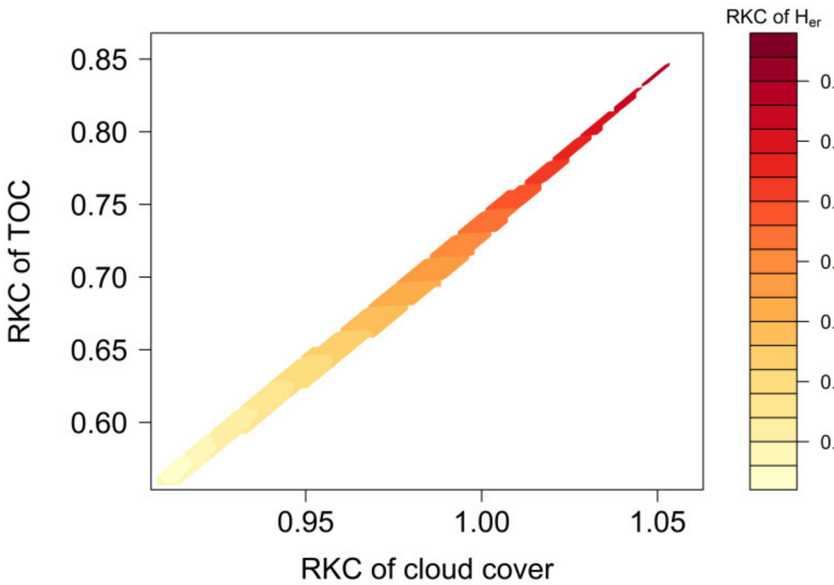

Figure 6. Dependence of running Kolmogorov complexity (RKC) of H_{er} from RKC of TOC and cloud cover for a fixed window of 100.

KC provides average information about the complexity of the H_{er} time series since its complexity has remained hidden in the rules of the applied procedure. Therefore, to obtain information about the randomness of each amplitude in the H_{er} time series, using all samples representing the time series, we presented the KC spectrum and its spectrum highest value (KCH). Figure 7 depicts the KC complexity spectrum of the normalized H_{er} for different years. Inspection of this figure reveals that the distribution of years regarding the order of KCH is similar to those grouped pursuing the order of KC values. If we exclude 2003 because the time series is shorter (starting from April), the highest KCH was in the period 2004–2006 (from 0.535 to 0.583) and 2011 (0.559). However, in 2011 KCH was above the average although KC was not high (0.349). The high KCH in 2011 occurred at H_{er} values between 2700 and 2900 Jm^{-2}, which were most commonly recorded in September 2011.

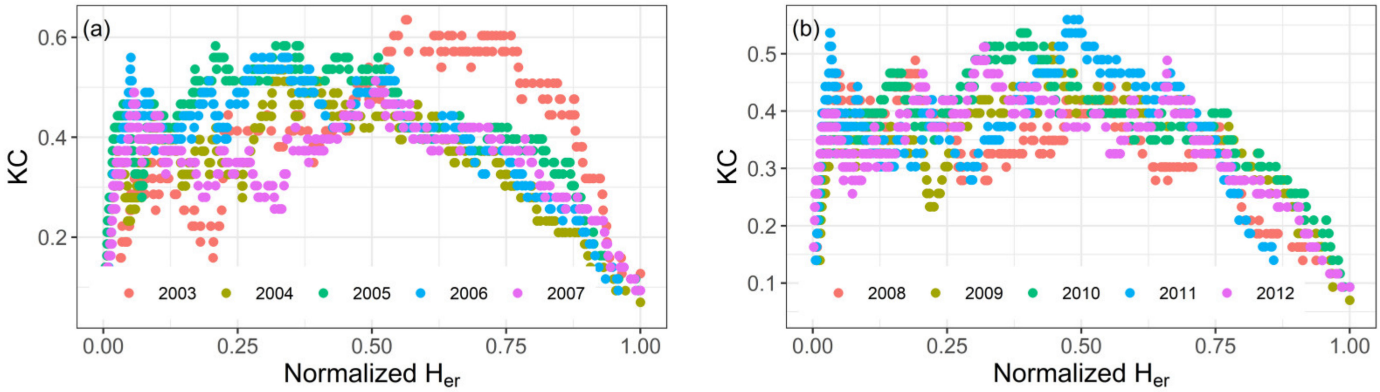

Figure 7. Kolmogorov complexity spectra of the daily H_{er} time-series in Novi Sad for (**a**) period 2003-2007 and (**b**) period 2008-2012.

Figure 8 shows values of the KC spectrum sorted in ascending order of the observed variable. From Figure 8a can be noticed that the highest values of the KC spectrum are in the range between 2500 and 3500 Jm^{-2}, which are values usually recorded in spring (April and May) and late summer and beginning of autumn (second half of August and September). Figure 8a also reveals that up to H_{er} value of approximately 1100 Jm^{-2} the KC spectrum exhibits considerable variability, while at higher H_{er} values the KC spectrum is smoother. Since the highest frequencies have H_{er} values less than 1100 Jm^{-2} (Figure 2), this indicates that low H_{er} values disturb the smoothness of the spectrum. The KCH of the TOC data was observed in the TOC range between 320 and 330 DU, values commonly observed in January and July. The KCH of cloud cover is high in the range of 3–8 tenths. These partly cloudy conditions have a strong influence on the variability of daily H_{er} values because of the uncertainty of whether the sun disk is covered by the cloud or not. Additionally, under partly cloudy conditions multiple scattering between the upper and lower clouds may contribute to the complexity of the H_{er} values. Under conditions of low cloud cover (0–2 tenths), there is a high probability that the sun will not be obstructed by clouds. Similarly, under conditions of high cloud cover (9–10 tenths), complete sun obstruction is most likely. Therefore, both low and high cloud cover conditions can reduce the complexity of H_{er} values.

In the extension to the previous analysis, we have compared the KCH obtained with the spectral method and the KC obtained with the mean used as the threshold amplitude. As mentioned, KCH could be considered a better indicator of complexity than KC, which is not always an appropriate measure of complexity. This is especially amplified in the case of asymmetric distributions [27]. Figure 9 shows that over the period 2004–2006 and 2010, KC and KCH values are high and similar. These are the years when the H_{er} values were the lowest, confirming the earlier conclusion that low H_{er} values disturb the smoothness of the spectrum. On the other hand, during the years when H_{er} values were higher (2007–2009, 2011–2012), KCH showed that time series of daily H_{er} were much more complex than it is shown by KC.

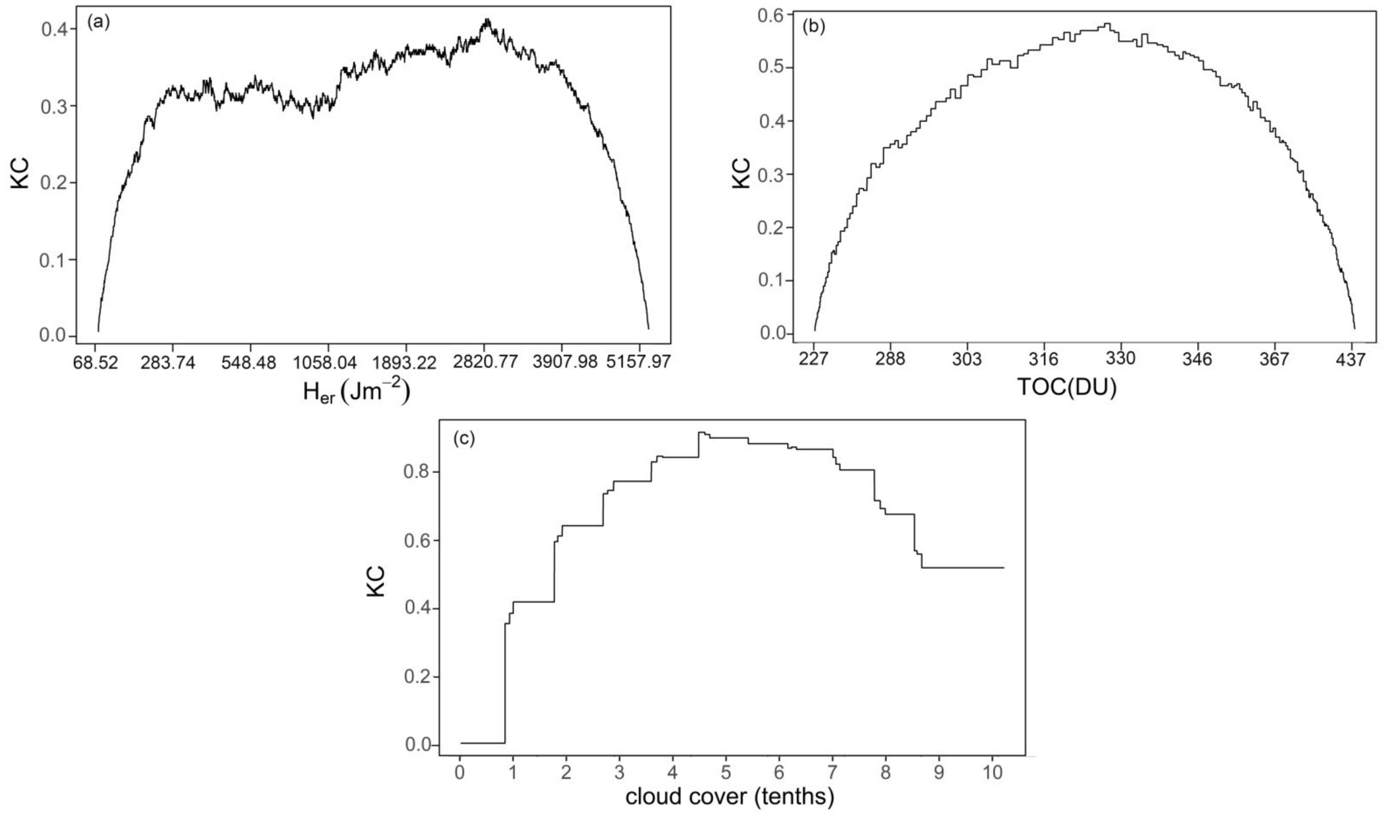

Figure 8. KC spectrum of (**a**) H_{er}, (**b**) TOC, and (**c**) cloud cover spectrum sorted in ascending order of the observed variable of the daily H_{er} time-series in Novi Sad.

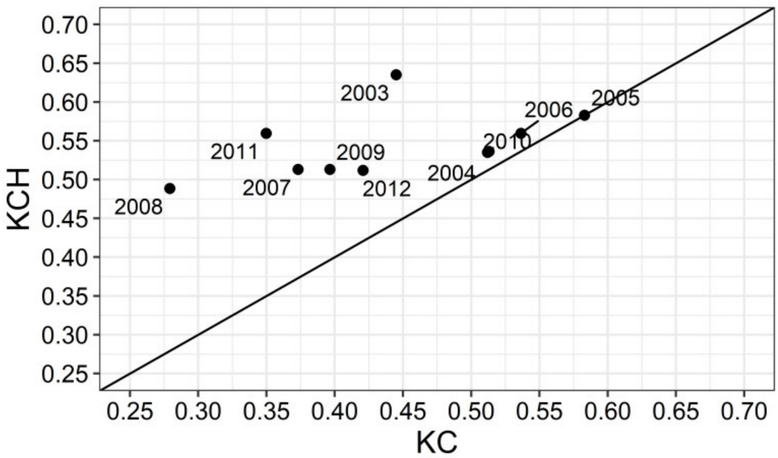

Figure 9. Kolmogorov complexity (KC) and the highest value in the Kolmogorov complexity spectrum (KCH) of the daily H_{er} time-series in Novi Sad.

3.3. Largest Lyapunov Exponent and Predictability of Daily H_{er}

Although the words "random" and "chaotic" are often considered synonymous, they do not have the same meaning. Randomness has no order and does not follow any pattern, while chaotic systems are characterized by short-term predictability that deteriorates rapidly over time. As we mentioned earlier, one of the indicators of chaotic behavior is the Lyapunov exponent whose positive values indicate the presence of chaos.

Figure 10a shows that H_{er} time-series exhibit low chaotic behavior ($0.030 \leq$ LLE ≤ 0.100) and moderate randomness ($0.350 \leq$ KC ≤ 0.583). Generally, years with higher values of

H_{er} exhibited higher chaotic behavior and lower randomness and vice versa. The more chaotic behavior of higher H_{er} values that occur in conditions of lower cloudiness shows that they are also more predictable. Simple inspection of Figure 10b indicates that the lowest predictability was for the years 2003, 2007, 2008, and 2011 (between 10 and 15 days), while during the rest of the years, predictability was between 20 and 33 days.

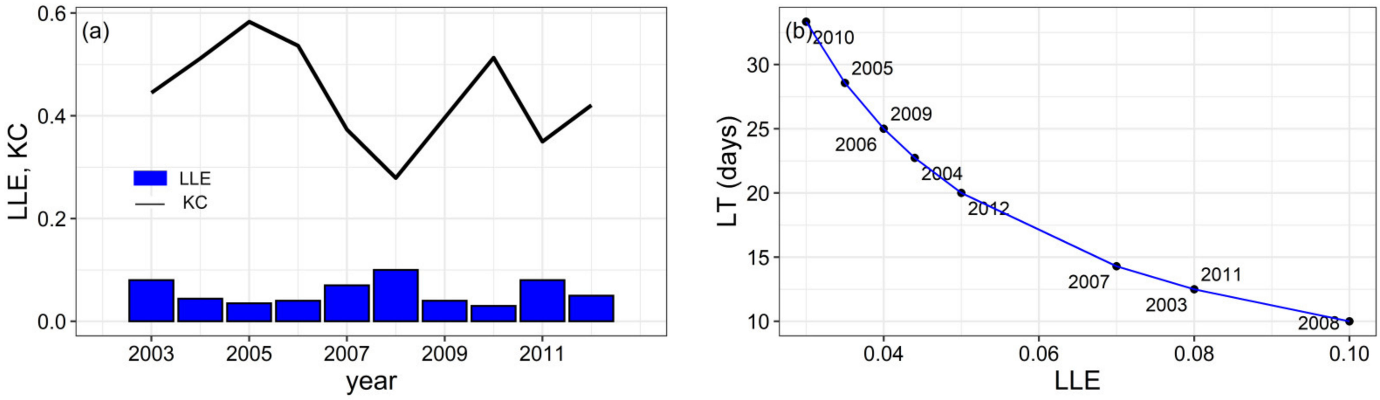

Figure 10. (**a**) Largest Lyapunov exponent (LLE) and Kolmogorov complexity (KC), and (**b**) LLE versus Lyapunov time (LT) of daily H_{er} time-series in Novi Sad.

While LT represents the approximate time limit for which accurate prediction for a chaotic system is possible, KT is estimated to be proportional to its randomness. Therefore, if KC is low (tends to 0), KT tends to ∞ and accurate long-term predictions are reasonable, while if KC is high only short-term predictions can be performed. The Lyapunov time was corrected for the presence of randomness since the chaos theory generally deals with the "irregular behavior in a complex system that is generated by nonlinear deterministic interactions with only a few degrees of freedom, where noise or intrinsic randomness does not play an important role" [54]. Therefore, the LT of daily H_{er} time-series is corrected for randomness by Kolmogorov as $[0, \mathrm{LT}] \cap [0, \mathrm{KT}]$, and it is presented in Figure 11a. This figure shows that the prediction effect of KT for KC is between 1.5 and 3.5 days, while for KCH is between 1.5 and 2.0 days. Figure 11b shows power law dependence between shows LT and KT. How much the randomness can reduce the LT can be seen from the comparison of Figures 10b and 11b. According to Figure 10b, the longest predictability in the LT units for daily H_{er} time-series was around 33 days while following from the fit on Figure 11b the presence of randomness reduced that number to 28 days.

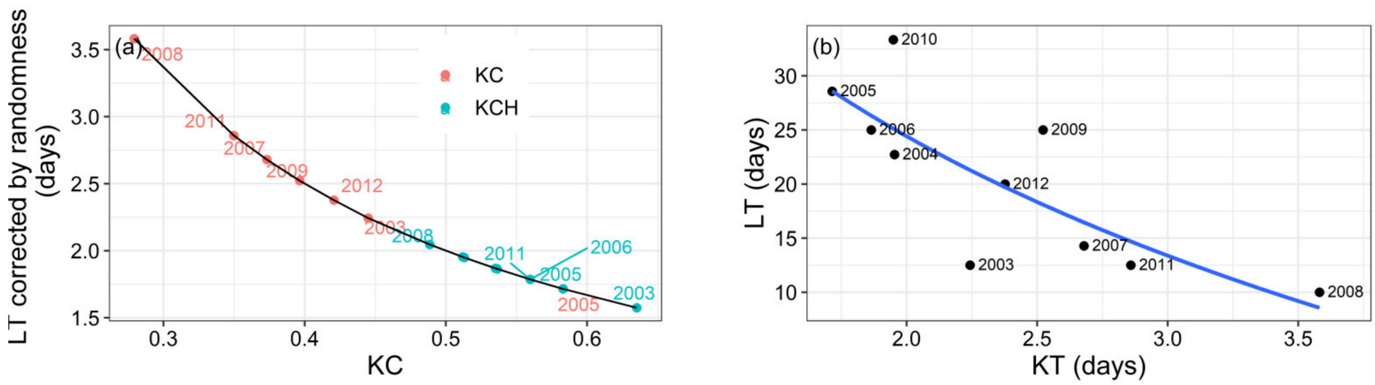

Figure 11. (**a**) Predictability of the daily H_{er} data in Novi Sad given by the Lyapunov time (LT, in days) corrected by randomness versus Kolmogorov complexity (KC), and (**b**) LT versus Kolmogorov time (KT, in days).

4. Conclusions

In this study, we analyzed the complexity and predictability of the daily erythemal dose (H_{er}) data recorded in Novi Sad (Serbia) from April 2003 to December 2012. For that purpose, we used the Kolmogorov complexity and related complexity measures (Kolmogorov complexity spectrum and its highest value, running Kolmogorov complexity, and Kolmogorov time), largest Lyapunov exponent, and Lyapunov time. The result reveals that fluctuations in daily H_{er} are moderate random and exhibit low chaotic behavior. According to Mihailovic et al. [30], complexity is a measure of randomness that conceptually reflects the number of occurrences of positive–negative or negative–positive deviation of the daily incident solar energy from the threshold. Our analysis indicated that daily H_{er} time series show a tendency to increase the randomness as the randomness of cloud cover and TOC increases, affecting the short-term predictability. We found a higher number of positive–negative or negative–positive deviations from the mean in time series over the years with lower values of H_{er} (2007–2009, 2011–2012), which explains the higher complexity. Conversely, time series over the years with higher values of H_{er} showed lower randomness and higher chaotic behavior. Analysis of the KC spectrum showed that at lower H_{er} values (up to approximately 1100 Jm^{-2}) the KC spectrum shows considerable variability, while at higher H_{er} values the KC spectrum is smoother indicating that low H_{er} values disturb the smoothness of the spectrum. The prediction horizon of daily H_{er} values in Novi Sad given by the Lyapunov time corrected for randomness by Kolmogorov, is between 1.5 and 3.5 days.

Author Contributions: Conceptualization, D.T.M., S.M.-M., and A.M.; methodology, D.T.M., A.M., and S.M.-M.; software D.T.M., A.M., and S.M.-M.; validation, D.T.M., S.M.-M., and A.M.; formal analysis, S.M.-M., A.M., and D.T.M.; investigation, S.M.-M., A.M., and D.T.M.; resources, A.M., D.T.M., and S.M.-M.; data curation, S.M.-M.; writing—original draft preparation, S.M.-M.; writing—review and editing, D.T.M., and A.M.; visualization, S.M.-M.; supervision, D.T.M., and A.M.; project administration, D.T.M. and S.M.-M.; funding acquisition, D.T.M., S.M.-M., and A.M. All authors have read and agreed to the published version of the manuscript.

Funding: This work was supported by the Ministry of Education, Science and Technological Development of the Republic of Serbia (Contract No. 451-03-68/2022-14/200172).

Institutional Review Board Statement: Not applicable.

Informed Consent Statement: Not applicable.

Data Availability Statement: The data presented in this study are available on request from the corresponding author.

Acknowledgments: The UV radiation measurement in Novi Sad in the period 2003–2012 was supported by the City Administration for Environmental Protection—City of Novi Sad.

Conflicts of Interest: The authors declare no conflict of interest.

References

1. Farman, J.C.; Gardiner, B.G.; Shanklin, J.D. Large losses of total ozone in Antarctica reveal seasonal ClOx/NOx interaction. *Nature* **1985**, *315*, 207–210. [CrossRef]
2. *CIE International Lighting Vocabulary*; Commission Internationale de l'Eclairage (International commission on Illumination): Vienna, Austria, 1987; Publication No. 17.4.
3. Bukata, R.P.; Jerome, J.H.; Kondratyev, K.Y.; Pozdnyakov, D.V. *Optical Properties and Remote Sensing of Inland and Coastal Waters*; CRC Press: Boca Raton, FL, USA, 1995.
4. Kaurola, J.; Taalas, P.; Koskela, T.; Borkowski, J.; Josefsson, W. Long-term variations of UV-B doses at three stations in northern Europe. *J. Geophys. Res.* **2000**, *105*, 20813–20820. [CrossRef]
5. Smedley, A.R.D.; Rimmer, J.S.; Moore, D.; Toumi, R.; Webb, A.R. Total ozone and surface UV trends in the United Kingdom: 1979–2008. *Int. J. Climatol.* **2012**, *32*, 338–346. [CrossRef]
6. Petkov, B.; Vitale, V.; Di Carlo, P.; Mazzola, M.; Lupi, A.; Diémoz, H.; Fountoulakis, I.; Drofa, O.; Mastrangelo, D.; Casale, G.R.; et al. The 2020 Arctic ozone depletion and signs of its effect on the ozone column at lower latitudes. *Bull. Atmos. Sci. Technol.* **2021**, *2*, 8. [CrossRef]

7. *WMO Scientific Assessment of Ozone Depletion: 2018*; Global Ozone Research and Monitoring Project—Report No. 58; World Meteorological Organization: Geneva, Switzerland, 1987.
8. *UNEP Environmental Effects and Interactions of Stratospheric Ozone Depletion, UV Radiation, and Climate Change: 2018 Assessment Report*; Environmental Effects Assessment Panel (EEAP), United Nations Environment Programme (UNEP): Nairobi, Kenya, 2019.
9. Eleftheratos, K.; Kazadzis, S.; Zerefos, C.S.; Tourpali, K.; Meleti, C.; Balis, D.; Zyrichidou, I.; Lakkala, K.; Feister, U.; Koskela, T.; et al. Ozone and Spectroradiometric UV Changes in the Past 20 Years over High Latitudes. *Atmos.-Ocean* **2015**, *53*, 117–125. [CrossRef]
10. Fountoulakis, I.; Bais, A.F.; Fragkos, K.; Meleti, C.; Tourpali, K.; Zempila, M.M. Short- and long-term variability of spectral solar UV irradiance at Thessaloniki, Greece: Effects of changes in aerosols, total ozone and clouds. *Atmos. Chem. Phys.* **2016**, *16*, 2493–2505. [CrossRef]
11. Sanchez-Lorenzo, A.; Enriquez-Alonso, A.; Wild, M.; Trentmann, J.; Vicente-Serrano, S.M.; Sanchez-Romero, A.; Posselt, R.; Hakuba, M.Z. Trends in downward surface solar radiation from satellites and ground observations over Europe during 1983–2010. *Rem. Sens. Environ.* **2017**, *189*, 108–117. [CrossRef]
12. Zerefos, C.S.; Tourpali, K.; Eleftheratos, K.; Kazadzis, S.; Meleti, C.; Feister, U.; Heikkilä, A. Evidence of a possible turning point in solar UV-B over Canada, Europe and Japan. *Atmos. Chem. Phys.* **2012**, *12*, 2469–2477. [CrossRef]
13. De Bock, V.; De Backer, H.; Van Malderen, R.; Mangold, A.; Delcloo, A. Relations between erythemal UV dose, global solar radiation, total ozone column and aerosol optical depth at Uccle, Belgium. *Atmos. Chem. Phys.* **2014**, *14*, 12251–12270. [CrossRef]
14. Bornman, J.F.; Barnes, P.W.; Robson, T.M.; Robinson, S.A.; Jansen, M.A.K.; Ballaré, C.L.; Flint, S.D. Linkages between stratospheric ozone, UV radiation and climate change and their implications for terrestrial ecosystems. *Photochem. Photobiol. Sci.* **2019**, *18*, 681–716. [CrossRef]
15. Frey, L.; Bender, F.A.M.; Svensson, G. Cloud albedo changes in response to anthropogenic sulfate and non-sulfate aerosol forcings in CMIP5 models. *Atmos. Chem. Phys.* **2017**, *17*, 9145–9162. [CrossRef]
16. Sabburg, J.; Wong, J. The effect of clouds on enhancing UVB irradiance at the earth's surface: A one year study. *Geophys. Res. Lett.* **2000**, *27*, 3337–3340. [CrossRef]
17. Arola, A.; Kazadzis, S.; Krotkov, N.; Bais, A.; Gröbner, J.; Herman, J.R. Assessment of TOMS UV bias due to absorbing aerosols. *J. Geophys. Res.* **2005**, *110*, D23211. [CrossRef]
18. García, R.D.; Cachorro, V.E.; Cuevas, E.; Toledano, C.; Redondas, A.; Blumthaler, M.; Benounna, Y. Comparison of measured and modelled spectral UV irradiance at Izaña high mountain station: Estimation of the underlying effective albedo. *Int. J. Climatol.* **2016**, *36*, 377–388. [CrossRef]
19. Blumthaler, M.; Ambach, W. Solar UV-B albedo of various surfaces. *Photochem. Photobiol.* **1988**, *48*, 85–88. [CrossRef]
20. Krzyscin, J.W.; Eerme, K.; Janouch, M. Long-term variations of the UV-B radiation over Central Europe as derived from the reconstructed UV time series. *Ann. Geophys.* **2004**, *22*, 1473–1485. [CrossRef]
21. Fountoulakis, I.; Diémoz, H.; Siani, A.-M.; Laschewski, G.; Filippa, G.; Arola, A.; Bais, A.F.; De Backer, H.; Lakkala, K.; Webb, A.R.; et al. Solar UV Irradiance in a Changing Climate: Trends in Europe and the Significance of Spectral Monitoring in Italy. *Environments* **2020**, *7*, 1. [CrossRef]
22. Fountoulakis, I.; Diémoz, H.; Siani, A.M.; Di Sarra, A.; Meloni, D.; Sferlazzo, D.M. Variability and trends in surface solar spectral ultraviolet irradiance in Italy: On the influence of geopotential height and lower-stratospheric ozone. *Atmos. Chem. Phys.* **2021**, *21*, 18689–18705. [CrossRef]
23. Shannon, C. A mathematical theory of communication. *Bell Syst. Tech.* **1948**, *27*, 379–423. [CrossRef]
24. Mihailovic, D.T.; Aksentijevic, A.; Mihailovic, A. Mapping regularities in the solar irradiance data using complementary complexity measures. *Stoch. Environ. Res. Risk Assess.* **2021**, *35*, 1257–1272. [CrossRef]
25. Kolmogorov, A.N. Three approaches to the quantitative definition of information. *Probl. Inf. Transm.* **1965**, *1*, 1–7. [CrossRef]
26. Hitchcock, J.M.; Pavan, A.; Vinodchandran, N.V. Kolmogorov complexity in randomness extraction. *ACM Trans. Comput. Theory* **2011**, *3*, 1–12. [CrossRef]
27. Mihailovic, D.T.; Mimic, G.; Nikolic-Djoric, E.; Arsenic, I. Novel measures based on the Kolmogorov complexity for use in complex system behavior studies and time series analysis. *Open Phys.* **2015**, *13*, 1–14. [CrossRef]
28. Mihailović, D.; Malinović-Milićević, S.; Arsenić, I.; Drešković, N.; Bukosa, B. Kolmogorov complexity spectrum for use in analysis of of UV-B radiation time series. *Mod. Phys. Lett. B* **2013**, *27*, 1350194. [CrossRef]
29. Bessafi, M.; Mihailović, D.T.; Malinović-Milićević, S.; Mihailović, A.; Jumaux, G.; Bonnardot, F.; Fanchette, Y.; Chabriat, J.-P. (Spatial and Temporal Non-Linear Dynamics Analysis and Predictability of Solar Radiation Time Series for La Reunion Island (France). *Entropy* **2018**, *20*, 946. [CrossRef]
30. Mihailović, D.T.; Bessafi, M.; Marković, S.; Arsenic, I.; Malinović- Milićević, S.; Jeanty, P.; Delsaut, M.; Chabriat, J.-P.; Drešković, N.; Mihailović, A. Analysis of solar irradiation time series complexity and predictability by combining Kolmogorov measures and Hamming distance for La Reunion (France). *Entropy* **2018**, *20*, 570. [CrossRef]
31. Bessafi, M.; Mihailovic, D.T.; Li, P.; Mihailovic, A.; Chabriat, J.-P. Algorithmic Probability Method Versus Kolmogorov Complexity with No-Threshold Encoding Scheme for Short Time Series: An Analysis of Day-To-Day Hourly Solar Radiation Time Series over Tropical Western Indian Ocean. *Entropy* **2019**, *21*, 552. [CrossRef]
32. Beck, H.; Zimmermann, N.; McVicar, T.; Vergopolan, N.; Berg, A.; Wood, E.F. Present and future Köppen-Geiger climate classification maps at 1-km resolution. *Sci. Data* **2018**, *5*, 180214. [CrossRef]

33. *ISO/CIE 17166:2019 (E)*; CIE Erythema Reference Action Spectrum and Standard Erythema Dose. CIE Publications: Wien, Austria, 2019.
34. WHO (World Health Organization). *Global Solar UV Index: A Practical Guide*; World Health Organization and International Commission on Non-Ionizing Radiation Protection; World Health Organization: Geneva, Switzerland, 2002.
35. Vanicek, K.; Frei, T.; Litynska, Z.; Schmalwieser, A. *UV-Index for the Public: A Guide for Publication and Interpretation of Solar UV Index Forecasts for the Public, Prepared by the Working Group 4 of the COST-713 Action "UVB forecasting" Report*; European Union: Brussels, Belgium, 2000.
36. Yankee Environmental Systems, Inc. *UVB-1 UV Pyranometer, Installation and User Guide, 2000, version 2.0*; Yankee Environmental Systems, Inc.: Turners Falls, MA, USA, 2000; 44p.
37. *CIE S007E-1998*; CIE Erythema Reference Action Spectrum and Standard Erythema Dose. CIE Central Bureau: Vienna, Austria, 1998.
38. Malinović-Milićević, S.; Mijatović, Z.; Stanojević, G.; Radovanović, M.M.; Popović, V. Health risks of extended exposure to low-level UV radiation—An analysis of ground-based and satellite-derived data. *Sci. Total Environ.* **2022**, *831*, 154899. [CrossRef]
39. Malinović-Milićević, S.; Mijatović, Z.; Arsenić, I.; Podraščanin, Z.; Firanj Sremac, A.; Radovanović, M.; Drešković, N. The importance of ground-based and satellite observations for monitoring and estimation of UV radiation in Novi Sad (Serbia). *J. Geogr. Inst. Jovan Cvijic SASA* **2020**, *70*, 57–70. [CrossRef]
40. Diémoz, H.; Siani, A.M.; Casale, G.R.; di Sarra, A.; Serpillo, B.; Petkov, B.; Scaglione, S.; Bonino, A.; Facta, S.; Fedele, F.; et al. First national intercomparison of solar ultraviolet radiometers in Italy. *Atmos. Meas. Tech.* **2011**, *4*, 1689–1703. [CrossRef]
41. Hülsen, G.; Gröbner, J. Characterization and calibration of ultraviolet broadband radiometers measuring erythemally weighted irradiance. *Appl. Opt.* **2007**, *46*, 5877. [CrossRef] [PubMed]
42. Malinovic, S.; Mihailovic, D.T.; Kapor, D.; Mijatovic, Z.; Arsenic, I.D. NEOPLANTA: A Short Description of the First Serbian UV Index Model. *J. Appl. Meteorol. Climatol.* **2006**, *45*, 1171–1177. [CrossRef]
43. Malinovic-Milicevic, S.; Mihailovic, D.T.; Radovanovic, M.M. Reconstruction of the erythemal UV radiation data in Novi Sad (Serbia) using the NEOPLANTA parametric model. *Theor. Appl. Climatol.* **2015**, *12*, 131–138. [CrossRef]
44. Van der A, R.J.; Allaart, M.A.F.; Eskes, H.J. Extended and refined multi sensor reanalysis of total ozone for the period 1970–2012. *Atmos. Meas. Tech.* **2015**, *8*, 3021–3035. [CrossRef]
45. Van der A, R.J.; Allaart, M.A.F.; Eskes, H.J. *Multi-Sensor Reanalysis (MSR) of Total Ozone, Version 2. Dataset*; Royal Netherlands Meteorological Institute (KNMI): De Bilt, The Netherlands, 2015. [CrossRef]
46. Cover, T.M.; Thomas, J.A. *Elements of Information Theory*; Wiley: New York, NY, USA, 1991; p. 748.
47. Li, M.; Vitanyi, P. *An Introduction to Kolmogorov Complexity and Its Applications*; Springer: New York, NY, USA, 1997.
48. Ziv, J.; Lempel, A. Compression of individual sequences via variable-rate coding. *IEEE Trans. Inf. Theory* **1978**, *24*, 530–536. [CrossRef]
49. Hu, J.; Gao, J.; Principe, J.C. Analysis of biomedical signals by the Lempel-Ziv complexity: The effect of finite data size. *IEEE Trans. Biomed. Eng.* **2006**, *53*, 2606–2609. [CrossRef]
50. Adami, C. What is complexity? *Bioessays.* **2002**, *24*, 1085–1094. [CrossRef]
51. Boeing, G. Visual analysis of nonlinear dynamical systems: Chaos, fractals, self-similarity and the limits of prediction. *Systems* **2016**, *4*, 37. [CrossRef]
52. Rosenstein, M.T.; Collins, J.J.; De Luca, C.J. A practical method for calculating largest Lyapunov exponents from small data sets. *Phys. D* **1993**, *65*, 117–134. [CrossRef]
53. Liu, H.-F.; Dai, Z.-H.; Li, W.-F.; Gong, X.; Yu, Y.-H. Noise robust estimates of the largest Lyapunov exponent. *Phys. Lett. A* **2005**, *341*, 119–127. [CrossRef]
54. Mihailović, D.T.; Nikolić-Dorić, E.; Arsenić, I.; Malinović-Milićević, S.; Singh, V.P.; Stošić, T.; Stošić, B. Analysis of daily streamflow complexity by Kolmogorov measures and Lyapunov exponent. *Physica A* **2019**, *525*, 290–303. [CrossRef]
55. Frison, T.W.; Abarbanel, H.D.I. Ocean gravity waves: A nonlinear analysis of observations. *J. Geophys. Res.* **1997**, *102*, 1051–1059. [CrossRef]
56. Gutierrez, R.J.; Boehmke, B.C.; Bauer, K.W.; Saie, C.M.; Bihl, T.J. anomalyDetection: Implementation of augmented network log anomaly detection procedures. *R J.* **2017**, *9*, 354–365. [CrossRef]
57. Mann, H.B. Nonparametric tests against trend. *Econometrica* **1945**, *13*, 245–259. [CrossRef]
58. Sen, P.K. Estimates of the regression coefficient based on Kendall's tau. *J. Am. Stat. Assoc.* **1968**, *63*, 1379–1389. [CrossRef]
59. Kendall, M.G. *Rank Correlation Methods*; Griffin: London, UK, 1975.